PCCP

PAPER

Check for updates

Low oxidation state aluminum-containing cluster anions: LAlH− and LAln− (n = 2−4, L = N[Si(Me)3]2)

Xinxing Zhang, [iD] [a] Linjie Wang, [a] Georgia R. Montone, [b] Ann F. Gill, [b] Gerd Ganteför, [a] Bryan Eichhorn, [c] Anil K. Kandalam [iD] *[b] and Kit H. Bowen*[a]

Several low oxidation state aluminum-containing cluster anions, LAlH− and LAln− (n = 2−4, L = N[Si(Me)3]2), were produced *via* reactions between aluminum hydride cluster anions, AlxHy−, and hexamethyldisilazane (HMDS). These clusters were characterized by mass spectrometry, anion photoelectron spectroscopy, and density functional theory (DFT) based calculations. Agreement between the experimental and theoretical vertical detachment energies (VDEs) and adiabatic detachment energies (ADEs) validated the computed geometrical structures. Reactions between aluminum hydride cluster anions and ligands promise to be a new synthetic scheme for low oxidation state, ligated aluminum clusters.

Introduction

The renaissance that aluminum chemistry has been celebrating in recent years has resulted from the major advancements in its low oxidation states (OS),[1,2] which first started by the advent of low OS aluminum precursors such as AlX (X = Cl, Br, I, Cp*),[3–8] and then largely expanded by the utilization of various protective organic ligands.[9–31] Amongst these ligands, deprotonated penta-methylcyclopentadiene (Cp*) received special attention[17–31] because of its anionic and aromatic nature and vast utilization in synthesizing molecules such as the famous ferrocene.[32] These interesting Cp* protected low OS aluminum compounds include various structures such as rings and cages[24–27] and various stoichiometries such as aluminum-poor[28] or aluminum-rich clusters.[29–31] Recently, we extended the study of Cp*-ligated aluminum clusters into the gas phase by the reactions between aluminum hydride cluster anions (AlxHy−) and Cp*H. We reported the formation and the anion photoelectron spectra of three previously unknown cluster anions: Cp*AlnH−, n = 1–3.[32]

Another ligand, deprotonated hexamethyldisilazane (HMDS), with the formula N[Si(Me)3]2− (we write N[Si(Me)3]2 as L for short), draws our attention, because it is also widely used to synthesize protected low OS aluminum clusters, especially the large ones. This ligand, being isovalent to NH2−, has two lone pairs for ligation. Being large in size, it also protects the central metal clusters from outer environments. For example, cluster-like Al7,[9] Al12,[10] Al69,[11] and Al77[12] with various numbers of L ligands

were synthesized using different AlX precursors. The Al77 cluster[12] is especially interesting because it contains a central Al atom surrounded by three concentric polyhedral shells with 12, 44, and 20 Al atoms, respectively; the whole cluster is stabilized by 20 L ligands. Studies of such large clusters provide insights for the transition from molecular species to bulk metal.

Like our previous study with Cp*AlnH−,[32] in the present work, we extend the study of L-ligated aluminum clusters to the gas phase. We report the formation and the anion photo-electron spectra of four low OS Al containing cluster anions: LAlH− and LAln− (n = 2–4, L = N[Si(Me)3]2). These clusters were formed due to reactions of aluminum hydride cluster anions AlxHy− with HMDS in a beam-gas reaction cell. We also report density functional theory (DFT) based calculations, which were used to identify the lowest energy structures of the neutral and negatively charged systems. Comparisons between the experimental and theoretical vertical detachment energies (VDEs) and adiabatic detachment energies (ADEs) validated the computed geometrical structures.

Methods

Experimental

Aluminum hydride cluster anions, AlxHy−, were generated in a pulsed arc cluster ionization source (PACIS), which has been described in detail elsewhere.[33–36] This source has proven to be a powerful tool for generating metal hydrides and their anions.[37–45] Briefly, for a ∼30 μs duration, 150 V electric pulse was applied across an anode and a sample cathode, vaporizing aluminum atoms and forming a plasma. In the present case, the sample cathode was a 0.5'' diameter pure aluminum rod. About 200 psi of ultrahigh purity hydrogen gas was also

[a] *Department of Chemistry, Johns Hopkins University, Baltimore, MD 21218, USA. E-mail: akandalam@wcupa.edu*

[b] *Department of Physics, West Chester University of PA, West Chester, PA 19383, USA. E-mail: kbowen@jhu.edu*

[c] *Department of Chemistry, University of Maryland, College Park, MD 20742, USA*

This journal is © the Owner Societies 2017

Phys. Chem. Chem. Phys., 2017, **19**, 15541–15548 | **15541**

injected into the arc region through a pulsed valve. The hydrogen gas, which had been partially dissociated by the discharge, propelled the aluminum–hydrogen atom plasma mixture down a 3 cm long flow tube, where its constituents interacted and formed cluster anions.

The anions generated by this method then passed through a 5 mm-wide gap before entering the reaction cell. These cluster anions were not mass-selected. The reaction cell was a 10 cm long, 1 cm diameter tube with 2 mm diameter apertures on each end. These apertures helped to maintain a suitable concentration of reactants in the cell and to minimize back-flow. To introduce HMDS ligands into the reaction cell, 50 psi of HMDS-seeded, ultra-high purity helium was injected through an aperture on the side of the reaction cell by a second pulsed valve. This aperture was mounted on the downstream end of the cell in order to reduce back-flow. The resulting anionic reaction products continued to drift toward the extraction plates of the time-of-flight mass spectrometry portion of the apparatus, from where their mass spectra were recorded. Cluster anions of interest were then mass-selected and their photoelectron spectra recorded.

Anion photoelectron spectroscopy was conducted by crossing mass-selected, negative ions with fixed-energy photons and analyzing the energies of the resultant photodetached electrons. This technique is governed by the well-known energy-conserving relationship, $h\nu = EBE + EKE$, where $h\nu$, EBE, and EKE are the photon energy, electron binding energy (photodetachment transition energy), and the electron kinetic energy, respectively. Our photoelectron apparatus, which has been described elsewhere,[46,47] consists of several possible anion sources, a linear time-of-flight mass spectrometer, a mass gate, a momentum decelerator, a neodymium-doped yttrium aluminum garnet (Nd:YAG) laser operated in the third harmonic (355 nm) for photodetachment, and a magnetic bottle electron energy analyzer with a resolution of 35 meV at EKE = 1 eV. The photoelectron spectra were calibrated against the well-known photoelectron spectrum of Cu$^-$.[48]

Theoretical

The ground state geometries of neutral and negatively charged LAlH and LAl$_n$ (n = 2–4, L = N[Si(Me)$_3$]$_2$) systems were obtained by carrying out density functional theory (DFT) based calculations using the Gaussian09 code.[49] The hybrid gradient corrected exchange–correlation functional[50,51] (B3LYP) along with the 6-31+G(d,p) basis set was employed during the geometry optimization, while a larger basis set, 6-311++G(3df,3pd) was used to compute energies of the optimized structures. In the geometry optimization procedure, the energy convergence criterion was set to 10^{-9} Hartree, while the gradient was converged to 10^{-4} Hartree per Å.

The vertical detachment energies (VDE) and the higher energy transitions obtained from the theoretical calculations were compared with the corresponding measured values. The calculated vertical detachment energy (VDE) is the energy difference between the ground state anion and its corresponding neutral in the geometry of the anion. The adiabatic detachment

energy (ADE) is calculated as the energy difference between the lowest energy geometry of the anionic cluster and the structurally similar/identical isomer (nearest local minimum) of its neutral counterpart. The calculated ADEs of the lowest energy isomers of anion were compared to the onset (lowest electron binding energy) region of the anion photoelectron spectrum. As mentioned above, all the energies reported here are calculated at the B3LYP/6-311++G(3df,3pd) level using the geometries obtained at the B3LYP/6-31+G(d,p) level.

Results and discussion

Fig. 1(a) and (b) respectively present the anion mass spectra before and after reaction. In Fig. 1(a), several homologous aluminum hydride cluster anions, Al$_x$H$_y^-$, series are observed, i.e., those based on n = 2–8. This mass spectrum has been obtained hundreds of times in our lab. After injecting HMDS seeded in helium into the reaction cell, we observed the mass spectrum presented in Fig. 1(b). There, most Al$_x$H$_y^-$ ions are etched away, and residual intensities of unreacted aluminum hydride cluster anions, deprotonated HMDS, i.e. N[Si(Me)$_3$]$_2^-$ (L$^-$) and its fragments, share the spectrum with four product peaks, LAlH$^-$, LAl$_2^-$, LAl$_3^-$, and LAl$_4^-$. Unit mass resolution was attained for all species in both spectra.

Fig. 2 presents the photoelectron spectra of the four products, LAlH$^-$, LAl$_2^-$, LAl$_3^-$ and LAl$_4^-$, taken with a 355 nm wavelength laser beam, respectively. The electron binding energy (EBE) value corresponding to the peak position in the lowest EBE spectral band is the vertical detachment energy (VDE). The VDE is the
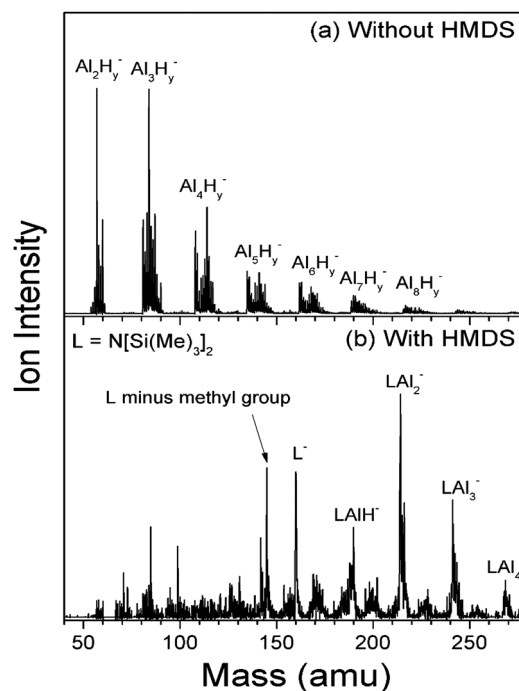

Fig. 1 (a) Mass spectrum of aluminum hydride cluster anions before reaction and (b) mass spectrum of L$^-$, LAlH$^-$, LAl$_2^-$, LAl$_3^-$ and LAl$_4^-$ after reaction (L = N[Si(Me)$_3$]$_2$).

15542 | *Phys. Chem. Chem. Phys.*, 2017, **19**, 15541–15548

This journal is © the Owner Societies 2017
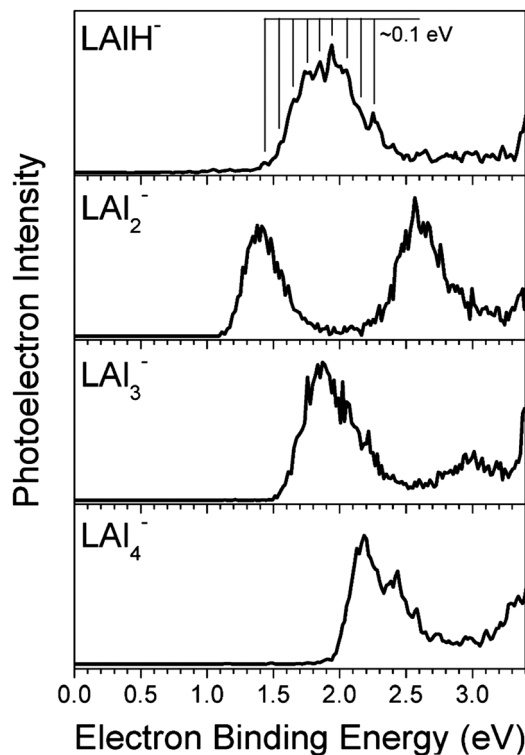
Fig. 2 Photoelectron spectra of LAlH⁻, LAl₂⁻, LAl₃⁻ and LAl₄⁻ anions recorded with 3.49 eV photons (L = N[Si(Me)₃]₂).

Fig. 3 Calculated structures of LAlH$^{-/0}$ isomers. Also shown are their relative energies in eV (L = N[Si(Me)₃]₂).

photo-detachment transition energy at which the Franck–Condon overlap between the wave functions of the anion and its neutral counterpart is maximal. The electron affinity (EA) is the energy difference between the lowest energy state of the anion and the lowest energy state of its neutral counterpart. When sufficient Franck–Condon overlap exists between $v = 0$ of the anion and $v' = 0$ of its corresponding neutral counterpart (the origin transition), and when no vibrational hot bands (photoelectrons from vibrationally excited anions) are present, the EA value corresponds to the EBE value at the intensity threshold of the lowest EBE band. Here, we have assigned EA values by extrapolating the low EBE side of the lowest EBE bands to zero. Adiabatic detachment energy (ADE) is the energy difference between a certain anionic isomer and its neutral counterpart relaxed to the nearest local minima.

With the above in mind, we observe that the spectrum of LAlH⁻ possesses a broad EBE band starting from around 1.4 eV and peaking at 1.85 eV. Hence, the experimental EA and VDE are determined to be 1.4 eV and 1.85 eV respectively. Embedded in this EBE band, we also observe a vibrational progression with a frequency of ∼0.1 eV corresponding to the Al–N stretching mode. The calculated structures of the anionic and neutral LAlH complexes, along with their relative energies, are given in Fig. 3. The lowest energy structure of LAlH⁻ complex, isomer **3a**, consists of an AlH moiety inserted into one of the Si–C bonds of the ligand L and bonded to the N atom so that Al atom has a four-fold coordination. The insertion of Al atom into a chemical bond was not the first example of such observation by
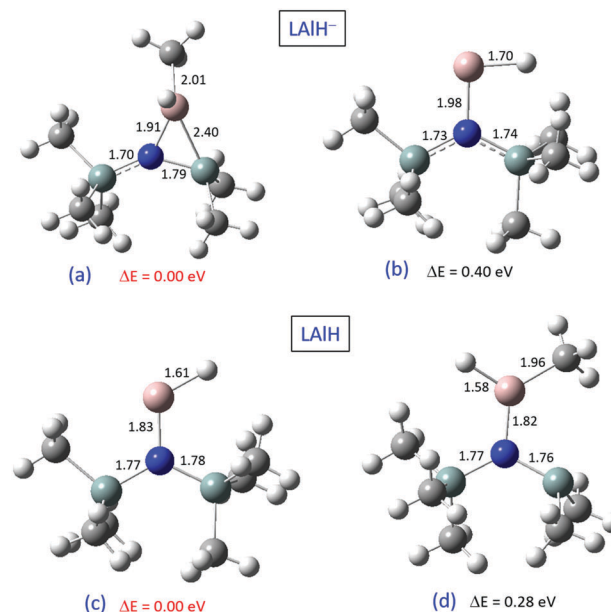
us; in the past we have observed Al insertion into a C–N bond.[52] In the higher energy isomer of the LAlH⁻ complex (isomer **3b**) on the other hand, the AlH moiety is bound only to the N atom of the ligand and no insertion into Si–C bond was observed. This isomer is 0.40 eV higher in energy than the Al-atom inserted structure, isomer **3a**. The calculated VDE of isomer **3a** is 2.83 eV (Table 1); however, there is no significant photoelectron signal at this energy in the photoelectron spectrum (Fig. 2). Interestingly, the calculated VDE of the higher energy isomer **3b** is 1.81 eV, which is in excellent agreement with the measured VDE value of 1.85 eV. In the case of the neutral LAlH complex, the energy ordering is reversed between the two isomers: the lowest energy structure of the neutral complex (isomer **3c**) is similar to the higher energy isomer of anionic LAlH⁻ (isomer **3b**), while the AlH-inserted structure (isomer **3d**), similar to the anionic ground state structure **3a**, is 0.28 eV higher in energy for the neutral system. The Al–N stretching frequency of neutral isomer **3c** is calculated to be 842 cm^{-1}, and is consistent with the experimental observation. The ADE, calculated as the energy difference between the lowest energy anion (isomer **3a**) and the structurally similar neutral system (isomer **3d**) is 1.95 eV, which is not in agreement with the measured value of 1.40 eV. On the other hand, the ADE value calculated as the energy difference between the anion's higher

Table 1 Experimentally measured ADE, VDE values and calculated ADE and VDE values. All numbers are in eV

Systems	Expt. ADE	Theo. ADE	Expt. VDE	Theo. VDE
LAlH⁻	1.40	1.30	1.85	1.81 (isomer **3b**)
LAl₂⁻	1.15	1.17	1.43	1.60 (isomer **4a**)
LAl₃⁻	1.60	1.72	1.89	2.04 (isomer **5a**), 1.73 (isomer **5b**)
LAl₄⁻	1.95	1.97	2.15	1.99 (isomer **6a**)

energy isomer (isomer **3b**) and its structural counterpart in the neutral (isomer **3c**) is 1.30 eV which is in good agreement with the experimental value of 1.40 eV. Thus, based on the agreement between the calculated VDE/ADE values of isomer **3b** with the measured values of VDE/ADE, it is concluded that it is the higher energy isomer of LAlH$^-$ that is present in the cluster beam of our experiment, but not the lowest energy isomer **3a**. The absence of the lowest energy isomer (isomer **3a**) in the cluster beam suggests that the neutral cluster (isomer **3c**) is formed first, and an electron binds to this neutral isomer to form the anion (isomer **3b**), from which the electron is photodetached later during the anion photoelectron spectroscopy.

The photoelectron spectrum of LAl$_2^-$ has two major EBE bands, the first one starting from 1.15 eV and peaking at 1.43 eV and the second one peaking at 2.60 eV. For LAl$_2^-$, our calculations reveal three nearly degenerate (within 0.30 eV) anionic structures (Fig. 4(a–c)). In the ground state structure, isomer **4a**, one aluminum atom of the Al$_2$ moiety is bound to the N atom while the other Al atom is inserted into one of the Si–C bonds of the ligand. The distance between the two aluminum atoms is 2.89 Å as compared to 2.70 Å in Al$_2$, suggesting a weak interaction between the aluminum atoms. On the other hand, in the second isomer, **4b**, both aluminum atoms are inserted into opposite Si–C bonds of the ligand, with an Al–Al bond length of 2.49 Å. The third isomer, **4c**, is 0.23 eV higher in energy and the entire Al$_2$ moiety is inserted into a single Si–C bond. Here, the proximal Al atom is triply coordinated with the Si, N and the distal Al atom, which is also bound to a terminal CH$_3$ group. Interestingly, the isomers in which Al atoms are not inserted into the Si–C bonds of the ligands were found to be 0.50–0.60 eV higher in energy. The calculated VDE

value for the lowest energy isomer, **4a**, is 1.60 eV, which is in good agreement with the measured value of the first maximum (1.43 eV). The molecular orbital (MO) analysis of this isomer revealed that the HOMO corresponds to a bonding orbital, with bonding characteristics between the N–Al bond and the Si–Al–CH$_3$ group (in HOMO). On the other hand, the HOMO−1 is dominated by bonding between the Al–Al atoms and N–Si atoms. Additionally, the calculated VDE value for isomer **4b** is 2.71 eV, which coincides with the second maximum (2.60 eV) of the photoelectron spectrum of LAl$_2^-$. Together with the fact that isomer **4b** is only slightly higher in energy than isomer **4a** ($\Delta E = 0.13$ eV), indicates the presence of both isomers **4a** and **4b** in the cluster beam, with the former contributing towards the first EBE peak (1.43 eV) and the latter to the second EBE peak (2.60 eV) of the photoelectron spectrum. In the case of isomer **4c**, however, the calculated VDE is 1.95 eV and does not appear in the LAl$_2^-$ spectrum. Thus, we can rule out the possibility of the existence of the third isomer in our ion beam.

The three lowest energy structures of neutral LAl$_2$ are shown in Fig. 4[(d)–(f)]. The lowest energy isomer, **4d**, of the neutral LAl$_2$ is similar to its anionic counterpart (isomer **4a**), but with considerable rotation of the CH$_3$ groups. The largest angular adjustment occurs at the CH$_3$ to the inserted Al atom. In the neutral species, the methyl group bound to the inserted aluminum atom is rotated by 22°, thereby increasing the bond angle, $\angle$ Si–Al–CH$_3$ by 19% as compared to its anionic counterpart, isomer **4a**. The next higher energy isomer, **4e**, is 0.38 eV higher in energy than isomer **4d**, in which one Al atom is bound to the N atom while the second Al atom is inserted into a Si–C bond. The structure of the third neutral isomer, **4f** ($\Delta E = 0.70$ eV) is similar to the third-lowest energy isomer of the anion (isomer **4c**).
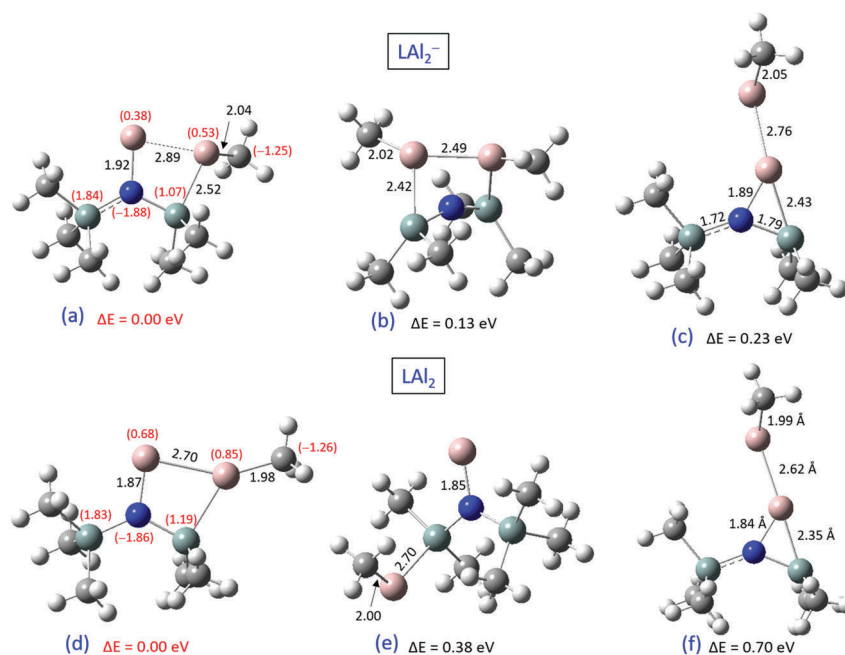
Fig. 4 Calculated structures of LAl$_2^{-/0}$ isomers. Also shown are their relative energies in eV (L = N[Si(Me)$_3$]$_2$). The NPA charges are given in the parentheses.

15544 | *Phys. Chem. Chem. Phys.*, 2017, **19**, 15541–15548

This journal is © the Owner Societies 2017

The ADE, 1.17 eV, is calculated as the energy difference between anionic isomer **4a** and its structurally similar neutral isomer **4d**. This is in good agreement with the measured EA (1.15 eV). Additionally, the broadening of the first EBE band in the photoelectron spectrum of LAl$_2^-$ can be attributed to the large structural adjustment that occurs in its lowest energy isomer (isomers **4a** vs. **4d**) during the photo-detachment process. The NPA charge analysis of isomer **4a** and its neutral analog, **4d**, shows that during photo-detachment of the electron from LAl$_2^-$ (isomer **4a**), the Al$_2$ moiety loses 65% of its charge, while the remaining 35% is lost from the CH$_3$ groups bound to and surrounding the inserted Al atom, the Si atom bound to the inserted Al atom and the N atom.

For the photoelectron spectrum of LAl$_3^-$, the onset of the first EBE band is around 1.6 eV, and the intensity maximum is 1.89 eV. More features beyond 2.5 eV can also be seen. The three lowest energy isomers of LAl$_3^-$ obtained from our calculations are shown in Fig. 5(a–c). Our calculations reveal three low lying isomers for the LAl$_3^-$ system (**5a–5c**). The ground state isomer, **5a**, can be viewed as an extension of the lowest energy isomer of LAl$_2^-$ (isomer **4a**), with the third atom of the Al$_3$ moiety added peripherally and coordinated with both the Al atom bound to the N and the inserted Al atom in isomer **4a**. The second anionic isomer, **5b**, has all three Al atoms bound to each other, forming a triangular Al$_3$ moiety with a single proximal Al atom bound to the N atom of the ligand, L. The third anionic structure, isomer **5c**, is 0.58 eV higher in energy and has all three Al atoms bound to each other in a linear fashion. The isomer **5c** can be considered as an expansion of **4b**, with the additional Al atom added between the two inserted Al atoms and bound to the N atom of the ligand, L. Overall, these structures indicate a growth pattern, where additional Al atoms

prefer to bond to each other as we go from LAl$_2^-$ to LAl$_3^-$. The calculated VDE for **5a** (2.04 eV) is in agreement with the measured value (1.89 eV). The HOMO of this isomer, from which the electron is photodetached, corresponds to a π bonding orbital located on the Al$_3$ moiety with a small anti-bonding interaction between N atom and the Al$_3$ moiety. The calculated VDE for isomer **5b** (1.73 eV) also falls within the first EBE band on the spectrum and is in reasonable agreement with the measured VDE value. Thus, despite being 0.20 eV higher in energy, the presence of **5b** in the cluster beam cannot be ruled out. Finally, in the case of isomer **5c**, the calculated VDE (1.33 eV) does not fall within the first EBE band on the LAl$_3^-$ spectrum. Overall, these calculated VDE values, together with the broadness of the first EBE on the spectrum, suggest the presence of both **5a** and **5b** in the cluster beam. Note that all electron detachment energies discussed above correspond to transitions from anionic doublet to neutral singlet states.

Our calculations show three nearly degenerate neutral structures for the LAl$_3$ complex (Fig. 5(d)–(f)). The lowest energy isomer, **5d**, is a neutral analog of the anion's lowest energy isomer, **5a**. The next isomer, **5e**, is 0.06 eV higher in energy and is structurally identical to the neutral higher energy isomer **5c**. Lastly, the third isomer, **5f**, is 0.13 eV higher in energy and is structurally analogous to the neutral isomer **5b**. The ADE of isomer **5a**, calculated as the energy difference between anionic isomer **5a** and its corresponding neutral isomer **5d**, is 1.72 eV, while the ADE of isomer **5b**, calculated as the energy difference between **5b** and its neutral analog (isomer **5f**), is 1.63 eV. The ADE values of isomers **5a** and **5b** are in good agreement with the measured EA value of 1.60 eV, thus reinforcing our earlier observation regarding the presence of both these isomers in the cluster beam. The NPA charge analysis of anionic isomer **5a** and
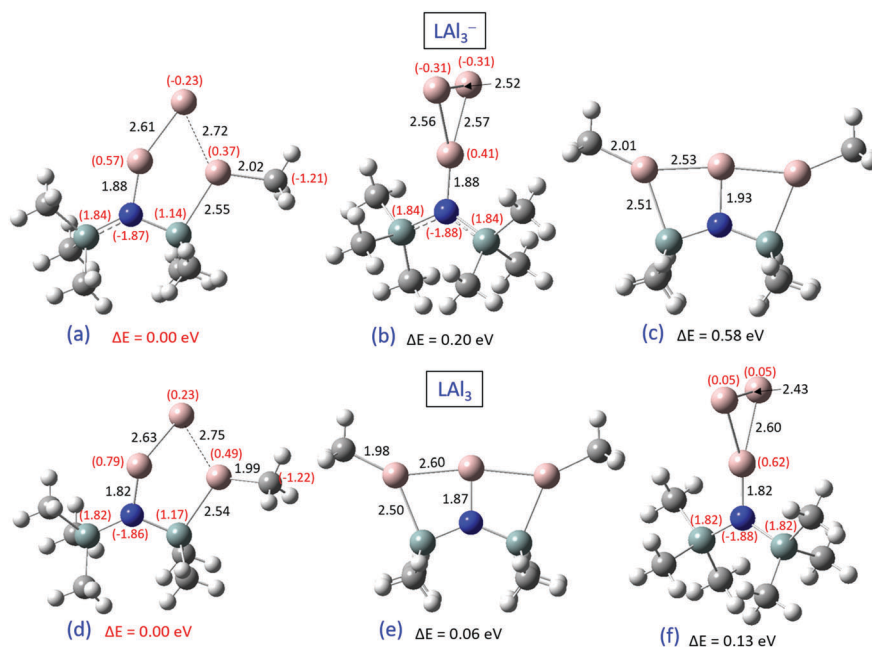

Fig. 5 Calculated structures of LAl$_3^{-/0}$ isomers. Also shown are their relative energies in eV (L = N[Si(Me)$_3$]$_2$). The NPA charges are given in the parentheses.
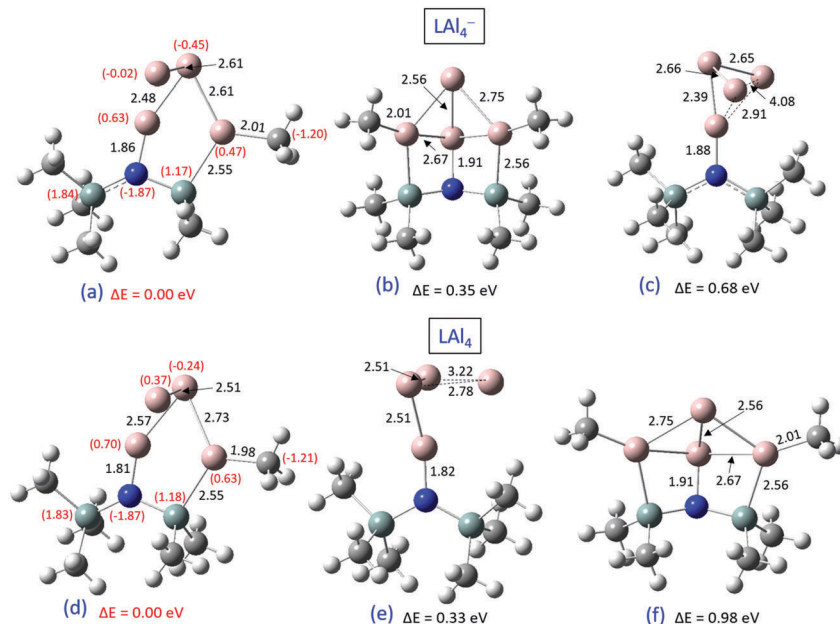
Fig. 6 Calculated structures of $LAl_4^{-/0}$ isomers. Also shown are their relative energies in eV (L = N[Si(Me)$_3$]$_2$). The NPA charges are given in the parentheses.

its neutral analog, **5d**, shows that during photo-detachment of the electron from the anion (**5a**), 82% of the electron's charge is lost by the Al$_3$ moiety. The remaining 18% is lost from the CH$_3$ groups bound to and surrounding the inserted Al atom, the Si atom bound to the inserted Al atom and the N atom.

The spectrum of LAl_4^- starts at 1.95 eV and peaks at 2.15 eV. In the case of LAl_4^-, our calculations reveal three low lying isomers (Fig. 6(a)–(c)). The ground state anionic structure, isomer **6a**, is an extension of the lowest energy isomer of LAl_3^- (isomer **5a**) with the fourth Al atom added peripherally to the distal Al atom of isomer **5a**. The second anionic isomer, **6b**, is 0.35 eV higher in energy and is also an extension of a low energy isomer of a smaller cluster size, isomer **5c**. Here, three Al atoms remain spanning the length of the ligand L while the fourth Al atom is peripherally coordinated with all three Al atoms, forming a broad pyramid-like moiety. The third isomer for anions, **6c**, is 0.68 eV and is an extension of **5b**, the second lowest energy structure of LAl_3^- system – with the fourth Al atom adding distally to the triangular Al$_3$ moiety resulting in a pyramidal Al$_4$ moiety. Again, the structures of these lower energy isomers demonstrate that the additional Al atoms prefer to maximize Al–Al interactions and add peripherally to the scaffolding of the lowest energy structures of the smaller complex, i.e., LAl_3^-. This suggests a continuation of the growth pattern as previously seen for the ground state of LAl_3^-. The calculated VDE for isomer **6a** (1.99 eV) is in reasonable agreement with the measured value (2.15 eV). For isomers **6b** and **6c**, the calculated VDEs are 2.60 eV and 1.81 eV, respectively. Even though, the calculated VDE of **6b** (2.60 eV) is not in agreement with the peak of the EBE band of the photo-electron spectrum, given the broadness of this band, ranging from 1.95 eV to 2.60 eV, one cannot rule out the possibility of the presence of isomer **6b**, along with isomer **6a**, in the cluster beam.

Calculations reveal three low energy structures for the neutral LAl$_4$ complex (Fig. 6(d)–(f)). The lowest energy isomer, **6d**, is structurally analogous to the anionic ground state isomer, **6a**. The second isomer, **6e**, is 0.33 eV higher in energy and its structure is similar to the anionic isomer, **6c**. However, in **6e**, the arrangement of the Al atoms of the Al$_4$ moiety is altered as one Al atom moves away from the proximal Al atom and interacts almost exclusively with the top two distal Al atoms – this disrupts the pyramidal geometry of the Al$_4$ moiety seen in its anionic counterpart, **6c**. The third isomer, **6f**, is 0.98 eV higher in energy. The structure of **6f** is similar to the anionic isomer, **6b** but displays some relaxation in the pyramid-like Al$_4$ moiety spanning the ligand, L. The ADE is calculated as the energy difference between anionic isomer **6a** and its corresponding neutral isomer **6d**, and has a value of 1.97 eV. This ADE is in excellent agreement with the measured EA value of 1.95 eV. As expected, the NPA charge analysis of the lowest energy isomers of the anionic and neutral LAl$_4$ complex reveal that during the photo-detachment of the extra electron, the Al$_4$ moiety loses majority (87%) of the charge, while 13% is lost from the CH$_3$ groups, Si, and N atoms of the ligand.

Concluding remarks

In this work, we generated four new clusters, LAlH$^-$, LAl$_2^-$, LAl$_3^-$ and LAl$_4^-$, from the reactions between aluminum hydride cluster anions and HMDS. We calculated their structures and electronic properties, and compared them with the experimental results. Very special structures, with Al atoms inserted into Si–C bond in a lot of cases, were found.

For aluminum, any oxidation states (OS) other than +3 and 0 are considered to be low OS. In this study, the (average) OS of

aluminum in the clusters LAlH$^-$, LAl$_2$$^-$, LAl$_3$$^-$, and LAl$_4$$^-$ are +1, 0, 0 and 0, respectively, given the conventional wisdom that the OS of L and H are both −1. The low oxidation states of aluminum in the clusters studied here make them not only prospective reagents for synthesis applications, but also potential energetic materials.

Acknowledgements

References

1 H. W. Roesky and S. S. Kumar, *Chem. Commun.*, 2005, 4027.
2 H. W. Roesky, *Inorg. Chem.*, 2004, **43**, 7284.
3 M. Tacke and H. Schnöckel, *Inorg. Chem.*, 1989, **28**, 2896.
4 M. Mocker, C. Rob and H. Schnöckel, *Angew. Chem.*, 1994, **106**, 1860.
5 A. Ecker and H. Schnöckel, *Z. Anorg. Allg. Chem.*, 1996, **622**, 149.
6 C. Dohmeier, C. Roble, M. Tacke and H. Schnöckel, *Angew. Chem.*, 1991, **103**, 594.
7 C. Dohmeier, D. Loos and H. Schnöckel, *Angew. Chem.*, 1996, **108**, 141.
8 J. Gauss, U. Schneider, R. Ahlrichs, C. Dohmeier and H. Schnöckel, *J. Am. Chem. Soc.*, 1993, **115**, 2402.
9 A. Purath, R. Köppe and H. Schnöckel, *Angew. Chem.*, 1999, **111**, 3114 (*Angew. Chem., Int. Ed.*, 1999, **38**, 2926).
10 A. Purath, R. Köppe and H. Schnöckel, *Chem. Commun.*, 1999, 1933.
11 H. Köhnlein, A. Purath, C. Klemp, E. Baum, I. Krossing, G. Stösser and H. Schnöckel, *Inorg. Chem.*, 2001, **40**, 4830.
12 E. Ecker, E. Weckert and H. Schnöckel, *Nature*, 1997, **387**, 379.
13 C. Dohmeier, M. Mocker, H. Schnöckel, A. Lötz, U. Schneider and R. Ahlrichs, *Angew. Chem.*, 1993, **105**, 1491 (*Angew. Chem. Int. Ed. Engl.*, 1993, **32**, 1428).
14 A. Schnepf and H. Schnöckel, *Adv. Organomet. Chem.*, 2001, **47**, 235.
15 C. Üffing, A. Ecker, R. Köppe, K. Merzweiler and H. Schnöckel, *Chem. – Eur. J.*, 1998, **4**, 2142.
16 N. Etkin and D. W. Stephan, *Organometallics*, 1998, **17**, 763.
17 S. J. Urwin, D. M. Rogers, G. S. Nichol and M. J. Cowley, *Dalton Trans.*, 2016, **45**, 13695.
18 A. Haaland, K.-G. Martinsen, S. A. Shlykov, H. V. Volden, C. Dohmeier and H. Schnöckel, *Organometallics*, 1995, **14**, 3116.
19 J. D. Gorden, A. Voigt, C. L. B. Macdonald, J. S. Silverman and A. H. Cowley, *J. Am. Chem. Soc.*, 2000, **122**, 950.
20 C. Dohmeier, H. Krautscheid and H. Schnöckel, *Angew. Chem.*, 1994, **106**, 2570.
21 C. Üffing, A. Ecker, R. Köppe and H. Schnöckel, *Organometallics*, 1998, **35**, 2373.
22 Q. Yu, A. Purat, A. Douchev and H. Schnöckel, *J. Organomet. Chem.*, 1999, **584**, 94.
23 J. Weiß, D. Stetzkamp, B. Nuber, R. A. Fischer, C. Boehme and G. Frenking, *Angew. Chem., Int. Ed. Engl.*, 1997, **36**, 70.
24 D. Weiß, T. Steinke, M. Winter, R. A. Fischer, N. Fröhlich, J. Uddin and G. Frenking, *Organometallics*, 2000, **19**, 4583.
25 S. Schulz, T. Schoop, H. W. Roesky, L. Häming, A. Steiner and R. Herbst-Irmer, *Angew. Chem., Int. Ed. Engl.*, 1995, **34**, 919.
26 C. K. F. von Haenish, C. Üffing, M. A. Junker, A. Ecker, B. O. Kneisel and H. Schnöckel, *Angew. Chem., Int. Ed. Engl.*, 1996, **35**, 2875.
27 C. Dohmeier, H. Schnöckel, C. Robl, U. Schneider and R. Ahlrichs, *Angew. Chem., Int. Ed. Engl.*, 1994, **33**, 199.
28 C. Ganesamoorthy, S. Loerke, C. Gemel, P. Jerabek, M. Winter, G. Frenking and R. A. Fischer, *Chem. Commun.*, 2013, **49**, 2858.
29 J. Vollet, J. R. Hartig and H. Schnöckel, *Angew. Chem., Int. Ed.*, 2004, **43**, 3186.
30 K. Weiß and H. Schnöckel, *Anal. Bioanal. Chem.*, 2003, **377**, 1098.
31 K. S. Williams and J. P. Hooper, *J. Phys. Chem. A*, 2011, **115**, 14100.
32 X. Zhang, G. Gantefoer, B. Eichhorn, D. Mayo, W. H. Sawyer, A. F. Gill, A. K. Kandalam, H. Schnöckel and K. Bowen, *J. Chem. Phys.*, 2016, **145**, 074305.
33 X. Zhang, Y. Wang, H. Wang, A. Lim, G. Gantefoer, K. H. Bowen, J. U. Reveles and S. N. Khanna, *J. Am. Chem. Soc.*, 2013, **135**, 4856.
34 X. Li, A. Grubisic, S. T. Stokes, J. Cordes, G. F. Gantefoer, K. H. Bowen, B. Kiran, M. Willis, P. Jena, R. Burgert and H. Schnoeckel, *Science*, 2007, **315**, 356.
35 X. Zhang, H. Wang, E. Collins, A. Lim, G. Ganteför, B. Kiran, H. Schnöckel, B. Eichhorn and K. H. Bowen, *J. Chem. Phys.*, 2013, **138**, 124303.
36 J. D. Graham, A. M. Buytendyk, X. Zhang, E. L. Collins, K. Boggavarapu, G. Gantefoer, B. W. Eichhorn, G. L. Gutsev, S. Behera, P. Jena and K. H. Bowen, *J. Phys. Chem. A*, 2014, **118**, 8158.
37 X. Zhang, G. Liu, G. Gantefoer, K. H. Bowen and A. N. Alexandrova, *J. Phys. Chem. Lett.*, 2014, **5**, 1596.
38 X. Zhang, P. Robinson, G. Gantefoer, A. Alexandrova and K. H. Bowen, *J. Chem. Phys.*, 2015, **143**, 094307.
39 A. Buytendyk, J. Graham, H. Wang, X. Zhang, E. Collins, Y. J. Ko, G. Gantefoer, B. Eichhorn, A. Regmi, K. Boggavarapu and K. H. Bowen, *Int. J. Mass Spectrom.*, 2014, **365–366**, 140.
40 H. Wang, X. Zhang, Y. Ko, G. F. Gantefor, K. H. Bowen, X. Li, K. Boggavarapu and A. Kandalam, *J. Chem. Phys.*, 2014, **140**, 164317.
41 X. Zhang, H. Wang, G. Ganterför, B. Eichhorn and K. Bowen, *Int. J. Mass Spectrom.*, 2016, **404**, 24.
42 X. Zhang, H. Wang, G. Ganteför, B. Eichhorn, B. Kiran and K. H. Bowen, *J. Chem. Phys.*, 2016, **145**, 154305.

43 V. Fontenot, B. Kiran, X. Zhang, H. Wang, G. Ganteför and K. H. Bowen, *Int. J. Mass Spectrom.*, 2016, **408**, 56.

44 X. Zhang, G. Liu, K.-H. Meiwes-Broer, G. Ganteför and K. H. Bowen, *Angew. Chem., Int. Ed.*, 2016, **55**, 1.

45 X. Zhang, G. Gantefoer, A. Alexandrova and K. H. Bowen, *Phys. Chem. Chem. Phys.*, 2016, **18**, 19345.

46 M. Gerhards, O. C. Thomas, J. M. Nilles, W. J. Zheng and K. H. Bowen, *J. Chem. Phys.*, 2002, **116**, 10247.

47 I. A. Popov, X. Zhang, B. W. Eichhorn, A. Boldyrev and K. H. Bowen, *Phys. Chem. Chem. Phys.*, 2015, **17**, 26079.

48 J. Ho, K. M. Ervin and W. C. Lineberger, *J. Chem. Phys.*, 1990, **93**, 6987.

49 M. J. Frisch, G. W. Trucks and H. B. Schlegel, *et al.*, *GAUSSIAN 09, Revision B.01*, Gaussian, Inc., Wallingford, CT, 2004.

50 A. D. Becke, *J. Chem. Phys.*, 1993, **98**, 5648.

51 C. Lee, W. Yang and R. G. Parr, *Phys. Rev. B: Condens. Matter Mater. Phys.*, 1988, **37**, 785.

52 X. Li, A. Grubisic, S. Eustis, D. Wang, T. Lectka, G. F. Gantefor, K. H. Bowen, R. Burgert and H. Schnockel, *Chem. Phys. Lett.*, 2009, **481**, 190.